ORIGINAL PAPER

Integrating molecular docking, DFT and CoMFA/CoMSIA approaches for a series of naphthoquinone fused cyclic α-aminophosphonates that act as novel topoisomerase II inhibitors

Yi Ma · Jian-Guo Wang · Bin Wang · Zheng-Ming Li

Abstract Since they are potential topoisomerase II (Topo II) inhibitors, naphthoquinone fused cyclic α-aminophosphonates display anticancer activity. In order to explore the inhibitory mechanisms of these compounds, they were docked into the active site of Topo II structure, which allowed their probable binding modes to be predicted. Some meaningful results concerning their structure–activity relationships were obtained from density functional theory calculations. Models based on quantitative comparative molecular field analysis and comparative molecular similarity index analysis were derived for the steric, electrostatic, hydrophobic and H-bonding features of the compounds. The present study provides valuable results that enhance our understanding of the anticancer activities of these inhibitors and will aid the rational drug design of novel Topo II inhibitors in the future.

Keywords QSAR · Topoisomerase II · Molecular docking · Anticancer activity · Rational drug design

Abbreviations

Topo II	Topoisomerase II
QSAR	Quantitative structure–activity relationships
DFT	Density functional theory
HOMO	Highest occupied molecular orbital
LUMO	Lowest unoccupied molecular orbital
ESP	Electrostatic potential
CoMFA	Comparative molecular field analysis
CoMSIA	Comparative molecular similarity index analysis

Introduction

Over the past few decades, targeted therapy has been a popular approach to the treatment of cancers or tumor-related diseases [1–4]. For instance, Tarceva binds to tyrosine kinase (TK) [5], WX-UK1 inhibits the urokinase-type plasminogen activator (U-PA) [6], and BAY43-9006 is an inhibitor that targets Raf kinase [7]. Among the various anticancer targets, DNA topoisomerase II (Topo II) has attracted much attention, and a number of inhibitors of it have been described [8–13]. Typical Topo II inhibitors include etoposide, doxorubicin, and mitoxantrone. Topo II is a nuclear enzyme in mammalian cells that interconverts topological isomers of DNA by breaking and resealing phosphodiester bonds. This enzyme modifies DNA linkages in two steps and is able to relax the supercoiled form of a circular, closed, double-stranded DNA molecule in the presence of an energetic cofactor such as ATP [14]. Topo II inhibitors that are known as "poisons" interact with DNA and/or topoisomerases to form stable ternary complexes, termed "cleavable complexes," which cause permanent DNA damage. This damage triggers a series

Y. Ma · J.-G. Wang (✉) · Z.-M. Li
State-key Laboratory and Institute of Elemento-Organic Chemistry, Nankai University,
Tianjin 300071, China
e-mail: nkwjg@nankai.edu.cn

B. Wang
College of Pharmaceutical Sciences, Nankai University,
Tianjin 300071, China

J.-G. Wang
Institute of Scientific Computing, Nankai University,
Tianjin 300071, China

of cellular events that ultimately induce apoptosis or other types of cell death [15].

Recently, Wang et al. reported that some naphthoquinone fused cyclic α-aminophosphonates exhibited significant antitumor activities on four human tumor cell lines, some of which were comparable to the bioactivity of doxorubicin. These compounds display their biological activities by interacting with human Topo II during preliminary assays [16]. In order to understand the molecular basis for the activities of these compounds, and to advance the design of novel inhibitors with enhanced potency and selectivity, detailed theoretical or computational studies are urgently needed. There are a number of works that describe QSAR studies of Topo II inhibitors [14, 17–20]. However, the structures of the compounds in these publications are quite different from the compounds in this study, and some of the QSAR investigations only utilized 2D-QSAR [19, 20]. Even in the publications that used 3D-QSAR, the studies were carried out in the absence of the receptor, and only traditional CoMFA/CoMSIA models were postulated [14, 17, 18]. To our knowledge, a number of Topo II crystal structures are now available in the PDB databank (http://www.rcsb.org/pdb/), and these provide new starting points for studies of the binding modes and the 3D-QSAR of Topo II inhibitors.

With these considerations in mind, we applied a combination of molecular docking approaches, DFT calculations and CoMFA/CoMSIA methods in order to explore the possible binding modes and elucidate the key structural and pharmacophoric requirements of these compounds.

Material and methods

Dataset and modeling

A total of 30 naphthoquinone fused cyclic α-aminophosphonate analogs were studied computationally. IC$_{50}$ data for these compounds have been obtained on four human tumor cell lines: A549 (human lung carcinoma), HeLa (human cervical carcinoma), HEp2 (human laryngeal carcinoma), and LoVo (human colon carcinoma) [16, 21]. Their chemical structures and antitumor data are shown in Table 1. In the SYBYL 6.91 program environment [22] running on an SGI 350 server and an SGI Fuel workstation, FlexX [23] and CoMFA/CoMSIA [24, 25] molecular modeling techniques were utilized to investigate the compounds of interest. The DFT computations were performed using the Gaussian 03 software package running on the NanKai-Star supercomputer [26]. The structures of the compounds were based on the crystal structure of compound **1** [16]. Gasteiger–Hückel charges were assigned to the structures, which were then minimized by the Tripos force field in a standard procedure until convergence to a maximum derivative of 0.001 kcal

mol^{-1} Å^{-1} was attained. All of the structures were stored in a molecular database.

FlexX docking

The crystal structure of Topo II (pdb entry 1ZXM) was retrieved from the pdb databank [27]. The amino acids in the protein were fixed in the "Biopolymer" module by correcting side chains, prolines and side-chain amides. FlexX is a fast automated docking program based on incremental construction, which considers ligand flexibility by changing the conformation of a small ligand molecule at the active site while keeping the protein rigid [23]. The crystal structure was stripped of water molecules, and hydrogen atoms were added in the standard geometry. Any amino acid residue within 6.5 Å of the cofactor AMP-PNP was considered to be in the binding pocket. CScore calculation was enabled and set to serial mode [28]. Database docking and the subsequent scoring procedures were performed using the default parameters of Sybyl 6.91.
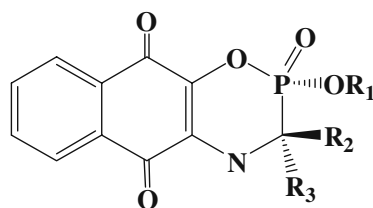
DFT calculations

Six representative structures(**1**, **4**, **6**, **15**, **17** and **21**) were chosen based on the results from FlexX for quantum chemical computational investigation. The conformers in the database of docking results had their single point energies calculated by the SCF method of density functional theory [29] (DFT) using the B3LYP function [30] with a basis set of 6-31 G(d) to describe their molecular properties. The conformations were not subjected to further structural optimization through quantum chemical computation since they were regarded as possible "bioactive conformations." All computations were conducted for the ground states of these molecules as single states. All of the convergent precisions used were the system's default values. The highest occupied molecular orbital (HOMO) and the electrostatic potential (ESP) were calculated precisely. Frequency analysis was performed, and net atomic charges were derived from a population analysis based on the NBO method. The atomic frontier electron density was defined as

$$f_i^E = \sum \left(C_{\text{HOMO},i} \right)^2 \times 100 \tag{1}$$

$$f_i^N = \sum \left(C_{\text{LOMO},i} \right)^2 \times 100, \tag{2}$$

where f_i^E is the electrophilic frontier electron density of atom i at the HOMO, and $C_{\text{HOMO},i}$ is the coefficient of the atomic orbital X_i in the HOMO. f_i^N is the nucleophilic frontier electron density of atom i at the LUMO, and $C_{\text{LOMO},i}$ is the coefficient of the atomic orbital X_i in the

Table 1 Molecular structures of the compounds under investigation and their antitumor activities ($-\log IC_{50}$) on four human tumor cell lines

compd	R_1	R_2	R_3	$-\log IC_{50}$ A549	$-\log IC_{50}$ HeLa	$-\log IC_{50}$ HEp2	$-\log IC_{50}$ LoVo
1	$-CH_3$	$-CH_3$	$-CH_3$	6.19	6.74	6.02	7.72
2	$-CH_3$	$-C_2H_5$	$-C_2H_5$	5.29	5.55	5.73	6.27
3	$-CH_3$	$-C_2H_5$	$-CH_3$	6.11	7.60	5.79	5.63
4	$-CH_3$	n-C_3H_7	$-CH_3$	5.16	5.11	4.97	5.22
5	$-CH_3$	n-C_4H_9	$-CH_3$	4.83	5.64	4.44	4.31
6	$-CH_3$	n-C_5H_{11}	$-CH_3$	4.24	4.18	4.76	4.17
7	$-CH_3$	n-C_6H_{13}	$-CH_3$	-	4.25	-	-
8	$-CH_3$	$-(CH_2)_4-$		4.83	4.17	4.44	-
9	$-CH_3$	$-(CH_2)_5-$		-	-	4.3	4.17
10	$-CH_3$	$-(CH_2)_6-$		-	4.18	4.09	-
11	$-CH_3$	-phenyl	-H	4.18	4.11	4.52	4.36
12	$-CH_3$	-H	-phenyl	4.06	4.21	4.36	4.12
13	$-CH_3$	o-nitrophenyl	-H	4.02	-	4.56	4.29
14	$-CH_3$	-H	o-nitrophenyl	3.99	-	4.33	4.17
15	$-C_2H_5$	$-CH_3$	$-CH_3$	5.58	6.19	5.29	6.09
16	$-C_2H_5$	$-C_2H_5$	$-C_2H_5$	4.92	4.32	4.78	4.28
17	$-C_2H_5$	$-C_2H_5$	$-CH_3$	4.85	4.57	4.8	4.25
18	$-C_2H_5$	n-C_3H_7	$-CH_3$	4.71	4.68	4.71	-
19	$-C_2H_5$	n-C_4H_9	$-CH_3$	4.57	-	-	4.05
20	$-C_2H_5$	n-C_5H_{11}	$-CH_3$	4.46	4.18	4.25	-
21	$-C_2H_5$	n-C_6H_{13}	$-CH_3$	4.25	-	-	-
22	$-C_2H_5$	$-(CH_2)_4-$		4.13	4.11	-	4.06
23	$-C_2H_5$	$-(CH_2)_5-$		-	-	4.3	4.11
24	$-C_2H_5$	$-(CH_2)_6-$		-	4.02	-	-
25	$-C_2H_5$	-phenyl	-H	4.09	4.26	4.34	4.19
26	$-C_2H_5$	-H	-phenyl	4	4.19	4.44	4.15
27	$-C_2H_5$	p-methoxyphenyl	-H	4.03	4.41	4.12	4.09
28	n-C_3H_7	$-CH_3$	$-CH_3$	5.08	4.79	4.76	4.9
29	n-C_3H_7	$-C_2H_5$	$-C_2H_5$	4.3	4.14	4.48	4.31
30	n-C_3H_7	$-(CH_2)_4-$		4.1	4.03	-	-

-data could not be obtained on the bioassay condition.

LUMO. f_i represents the reactivities of different atoms within a molecule.

CoMFA and CoMSIA study

CoMFA and CoMSIA can be used to explore the specific contributions of the steric, electrostatic, hydrophobic, and H-bonding factors that influence anticancer potency. For the CoMFA computation, the steric and electrostatic field energies were probed using an sp^3 carbon atom and a +1 point charge, respectively. Steric and electrostatic interactions were calculated using the standard Tripos force field with a distance-dependent dielectric constant of 5 employed at all intersections in a regularly spaced (2 Å) grid. The cutoff was set to 30 kcal mol^{-1} and column filtering was set to 2.0 kcal mol^{-1}. The "leave-one-out" (LOO) cross-validation method was applied to determine the optimum number of partial least squares (PLS) components. The optimum of six components was used in the non-cross-validated CoMFA model. The non-cross-validated models were assessed according to the variance explained r^2, the standard error of the estimated S, and the F ratio. The same dataset was also used to compute similarity index fields for CoMSIA analysis. CoMSIA similarity index descriptors (steric, electrostatic, hydrophobic, H-bond donor, and H-bond acceptor fields) were also calculated using a C1+ probe atom with a radius of 1.0 Å placed at grid spacing of 2 Å. The attenuation factor α was set to 0.3. The statistical evaluation in the CoMSIA analysis was carried out using the same procedure as described for the CoMFA computation. Contour plot levels for the CoMFA models were viewed at a threshold value of 88% for favored fields and a threshold value of 12% for disfavored fields. For the CoMSIA models, these data were 85% and 15% respectively.

Results and discussions

### Binding modes from the FlexX analysis

Until now, a human Topo II–inhibitor complex has not been reported. In a previous study, Leroy et al. concluded that the drug-binding site should be near the pocket where the ATP cofactor binds [31]. Presently, the best human Topo II crystal structure is 1ZXM [27], whose resolution is 1.87 Å. This structure is in a complex with AMP-PNP, an analog of ATP. Thus, in this study, we docked all 30 compounds in the database into the AMP-PNP binding cavity using FlexX (mostly employing the default settings). According to the database docking results, 13 of the 30 compounds could be closely superposed onto one another (**1**, **3**, **4**, **5**, **6**, **7**, **15**, **17**, **18**, **19**, **20**, **21**, **28**), and these compounds

exhibited similar conformations and orientations when binding in the same space with Topo II (Fig. 1). The FlexX scores ("total_score" in FlexX) for these 13 compounds were: −14.0, −14.5, −13.7, −11.4, −11.7, −10.5, −14.7, −14.4, −12.5, −13.0, −11.9, −10.5, and −14.1, respectively. The other 17 compounds failed to dock well with Topo II. We thus regard the conformations of these 13 compounds as the correct conformations. In theory, the FlexX total_score basically derives from the free energy of binding of the protein–ligand interaction [32]. We analyzed the biological activities (including the four IC$_{50}$ data series) of these compounds and their scores, and found that there are general monotonicities between the four sets of bioactivities and scores. The statistical r^2 for A549 activity (omitting compound **7**) and the FlexX score reaches 0.530 after a linear fit (Fig. 2). The statistical r^2 for the other three sets are below 0.5 and are thus ignored. Given the difference between the in vivo cell cytotoxic assays and the in vitro human Topo II inhibition assay, we can presume that the database docking was successful, and the molecular basis of the inhibition can be postulated. The A549 cell testing assay correlates best with the human Topo II binding energy.

The predicted binding modes are as shown in Fig. 3. Compound **1**, the best inhibitor in the series, is used to represent the interaction (the yellow molecule in Fig. 3a). The residues at the binding site include Glu87, Val90, Asn91, Ala92, Ala93, Asp94, Asn95, Lys96, Gln97, Arg98, Ile141, Leu146, Thr147, Ser148, Ser149, Asn150, Thr159, Gly160, Gly161, Arg162, Asn163, Gly164, Tyr165, Gly166, Ala167, and Lys168. According to a 2D view provided by LIGPLOT (Fig. 3b) [33], residues Asn91, Asp94, Thr147, Ser147, Gly161, Gly164, and Ala167 all directly interact with the inhibitor. Residues Asn91, Asp94, Thr147, and Gly164 are involved in hydrophobic interactions with the inhibitor. Three intermolecular H-bonds are formed between Asn91, Ser149, Ala167, and two oxygen atoms in compound **1**. All of the compounds have the same oxygen atoms in their structures, suggesting that they may undergo similar H-bonding interactions when they interact with Topo II. The phosphorus atom in the inhibitor occurs in a similar location to the phosphorus atom in the AMP-PNP structure (Fig. 3a). This indicates that the inhibitor compounds may compete with AMP-PNP when inhibiting Topo II.

The ESP (electrostatic potential) surface of the receptor is shown in Fig. 4a (this picture was taken by WebLab ViewPro [34]). It can be seen that the inhibitor is buried in a pocket surrounded by positive and negative potentials. We compared the ESP surface of the binding site with the ESP maps of compounds from DFT calculations. We found that the ESP surface of the inhibitor is quite a close fit to the ESP surface of the binding site. In the positively charged part of the binding pocket, the inhibitor has negative ESP;

Fig. 1 The 13 compounds (**1**, **3**, **4**, **5**, **6**, **7**, **15**, **17**, **18**, **19**, **20**, **21** and **28**), along with their correct docked conformations (based on FlexX results) when aligned in the binding site of the structure of Topo II (1ZXM)
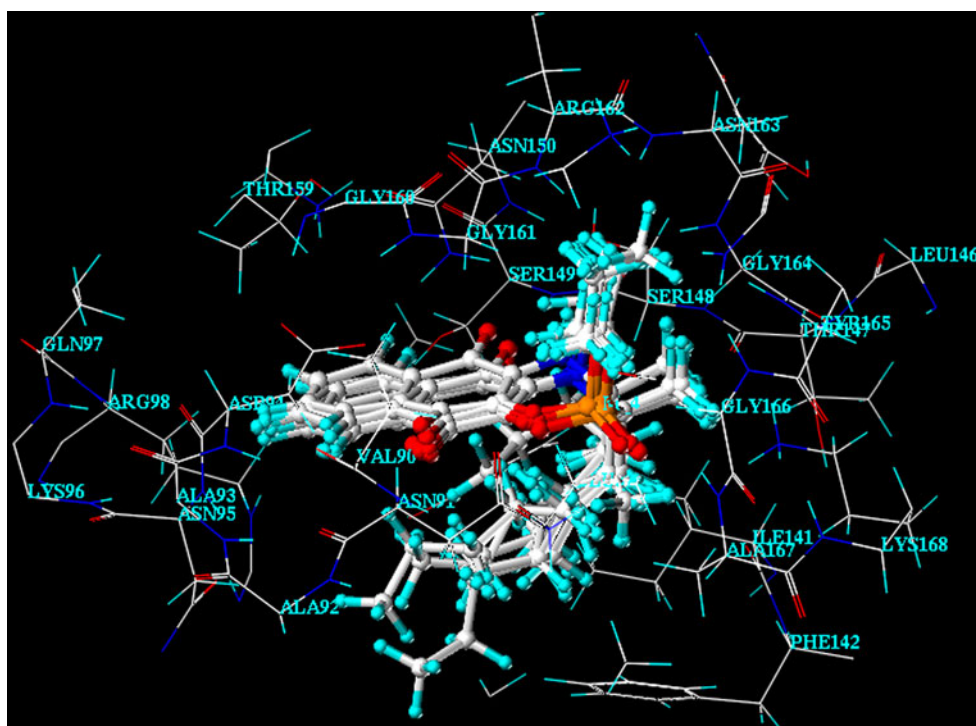
in the region where the compound displays positive ESP, the binding pocket has negative ESP.

From the above analysis, it can be assumed that the molecular docking was successful, even though only 13 of the 30 compounds gave the correct docking results, and the binding mode predicted by FlexX is suitable for elucidating the enzyme/inhibitor interaction and for aiding the design of new inhibitors.

ESP and MO features of the results of the DFT calculations

The DFT method has recently found widespread use in computational chemistry due to its desirable accuracy and

Fig. 2 FlexX score vs $-\log IC_{50}$(A549) for the 12 compounds (omitting compound **7**) in their correct docked conformations. The coefficient is 0.530

the fact that it is less demanding computationally than the classical ab initio method. In this study, six representative compounds were selected from the 13 compounds for DFT calculations. These compounds cover a range of A549 inhibition values from 4.57 to 6.19 (i.e., $-\log IC_{50}$), and vary in terms of their R_1 and R_2 substituents. People usually optimize the structures of compounds before describing their electrostatic and orbital properties. However, if bioactive conformations are already available, conformational optimization is not compulsory. Now that the docking results appear to be acceptable, there is good reason for submitting the conformations obtained by FlexX directly to theoretical calculations.

In recent years, many studies have indicated that the electrostatic potential and frontier molecular orbitals should be taken into account when investigating structure–activity relationships [35–38]. We calculated the frontier MO and the ESP of each of these six compounds by means of DFT/ B3LYP. The ESP maps of the compounds share significant similarities, and the ESP of compound 1 is shown in Fig. 4b (this graphic was generated by the program Molden [39]). As we mentioned above, the ESPs of the small molecules match the ESP of the human Topo II binding site perfectly, indicating that the docking conformation is close to the real bioactive conformation. The ESP maps of the six compounds are similar, with the negative moiety in the upper region and the positive part on the underside of each map. Based on the ESP distributions of the molecules, it is very possible that all of the compounds in the database interact with Topo II in a similar manner.
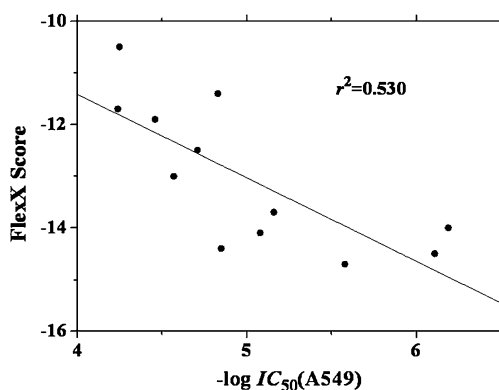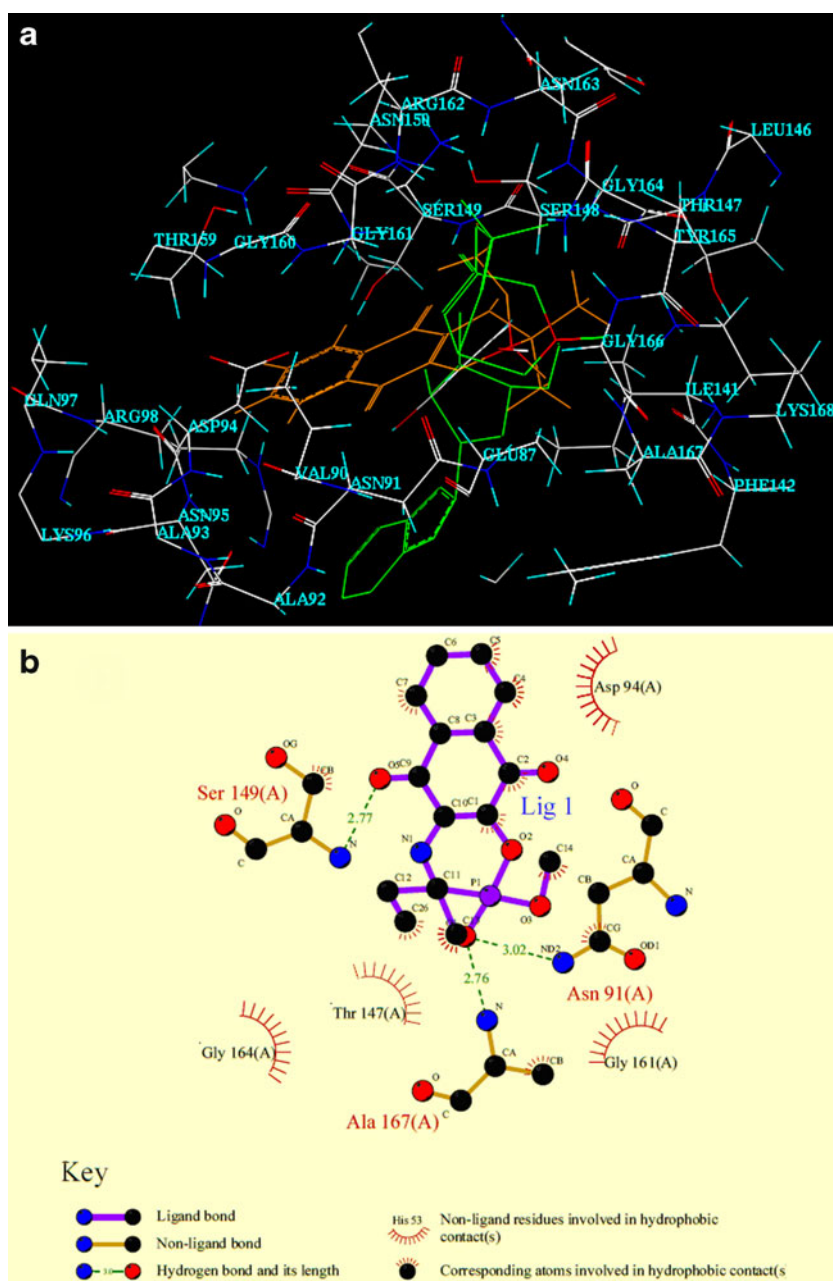
According to frontier molecular orbital theory, the HOMO and the LUMO are important factors that affect the bioactivities of small inhibitors. The HOMO mainly provides electrons, while LUMO mainly accepts them. In this study, we analyzed the HOMOs of the six typical compounds based on DFT single point energy calculations. Obvious differences are observed between the HOMOs of active and weakly active compounds. Compounds 1 and 4 are two potent inhibitors, and in each case the HOMO almost covers the whole molecule. Interestingly, for compounds 6, 15, 17 and 21, which are less active, the HOMO generally does not cover the aromatic phenyl ring in the naphthoquinone; it is spread mostly across the rest of the molecule. Only the HOMOs of compounds 1 and 21 are shown in order to simplify the figures (Fig. 5). From the interaction mode, π–π stacking is not evident, and there are numerous hydrophobic interactions. This implies that the hydrophobic interactions significantly affect the binding of the small compound to Topo II. The HOMO of the naphthoquinone fused cyclic α-aminophosphonate and the LUMOs of the surrounding residues contribute to the orbital interaction.

DFT calculations show that the HOMO has a strong impact on the bioactivity of the compound. At the same time, the electrostatic potential distribution needs to fit with the ESP of the surrounding pocket. These factors should be
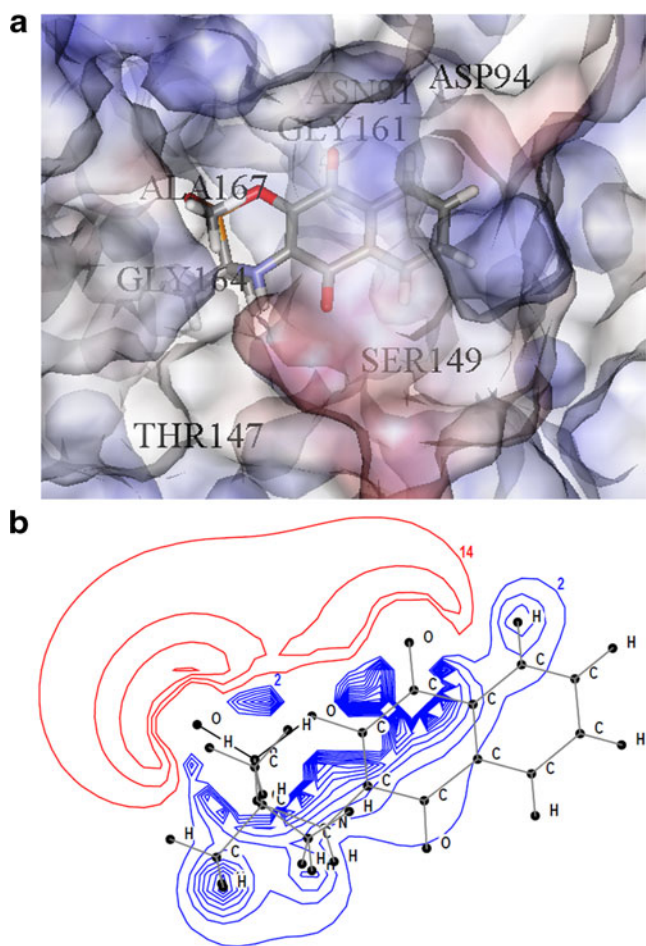
Fig. 4 a The 3D ESP (electrostatic potential) surface of the binding site of Topo II. **b** The 2D ESP surface of compound **1**, from DFT calculations. For the ESP, positively charged surfaces are shown in *blue*, and negatively charged surfaces are shown in *red*

compounds **2**, **5**, **7**, **13**, **25**, and **30** were random chosen for the test set, so the remaining compounds were treated as the training set. The test set was used to validate the predictive ability of the model derived from the training set. The robustness of the predictive power of the model was therefore assessed. For CoMSIA analysis, we did not separate the compounds into a training set and a test set, so all of the compounds with measurable activity were treated as the training set. It should be mentioned that for the CoMFA analysis of the HeLa data, compound **17** was omitted from the training set. The statistical results of all of these computations are summarized in Table 2. From the table, it can be seen that all the CoMFA/CoMSIA analyses yield satisfactory cross-validated q^2 values that range from 0.401 to 0.685, indicating that the 3D-QSAR models are predictive. The non-cross-validated r^2 values are all higher than 0.9, which shows that the final CoMFA/CoMSIA models are highly self-consistent. The quality of each CoMFA model was also checked by investigating its predictive ability for the compounds in the test set. The predicted bioactivities of the compounds in the test set were
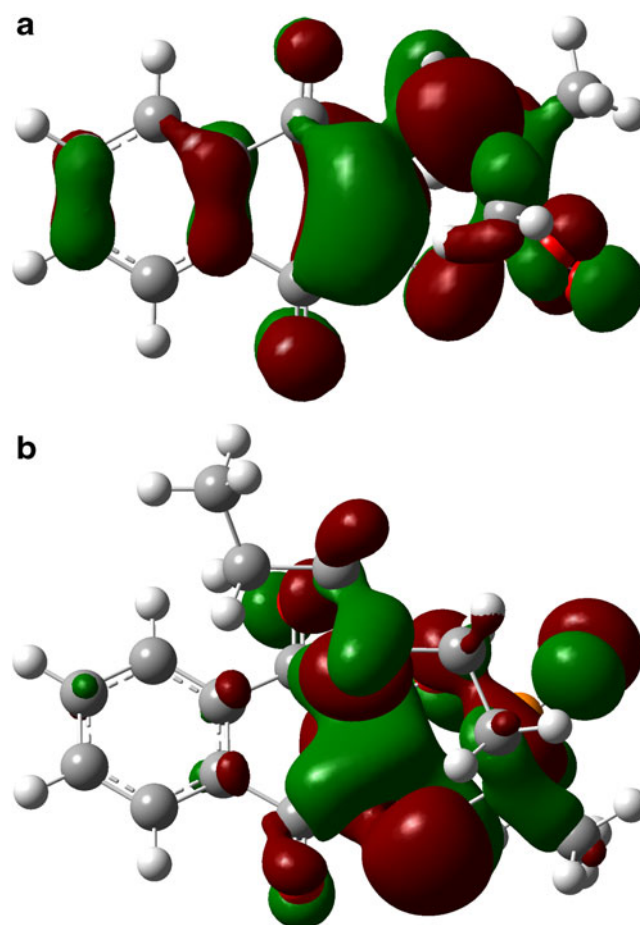

Fig. 5 a–b HOMO maps of compounds **1** (**a**) and **21** (**b**) from DFT calculations

taken into consideration when designing new compounds and studying the inhibition mechanism further.

3D-QSAR models

CoMFA and CoMSIA studies

Starting from the correct conformations obtained from FlexX, we fitted the other 17 compounds to the conformation of compound **1**. Comprehensive CoMFA and CoMSIA analyses were performed and the respective models were generated. As four sets of antitumor bioactivity data are available for this family of compounds, there should be some similarities among them. We thus developed CoMFA models for all four cell line bioactivity data sets. Since the A549 inhibition data showed the closest correlation with the FlexX score, we then built CoMSIA models for the A549 bioactivity dataset in order to investigate hydrophobicity and hydrogen bonding. For the CoMFA analyses,

Table 2 PLS statistics of the 3D-QSAR models for the cytotoxicities of naphthoquinone fused cyclic α-aminophosphonates

PLS statistics	CoMFA				CoMSIA
	A549	HeLa	HEp2	LoVo	A549
q^2	0.617	0.401	0.527	0.436	0.685
Components	5	6	3	3	5
r^2	0.964	0.989	0.936	0.964	0.919
S	0.157	0.138	0.157	0.227	0.212
F	57.603	157.809	31.853	49.383	33.876
Contribution					
Steric	0.93	0.956	0.921	0.877	0.306
Electrostatic	0.07	0.044	0.079	0.123	0.120
Hydrophobic					0.385
H-bond donor					0.115
H-bond acceptor					0.075

in general agreement with the experimental ones (data not shown).

Structure-based interpretation

The steric and electrostatic fields of the CoMFA contour maps are shown in Fig. 6. The four CoMFA models show strong similarities. This is in general agreement with our hypothesis that the four sets of anticancer activities may target the same enzyme. Thus, we only show the pictures of 3D contour maps derived from the A549 bioactivity dataset in this paper. The maps were fitted to the proposed binding site of human Topo II from the docking results in order to explain the model. All four CoMFA models presented large sterically favorable (green) areas in which bulky groups showed increased binding affinities. The green contours in the four models shared some common features, most of which occurred in the cavity formed by residues Phe142, Ser148, Ser149, Arg162, Asn163, Gly164, Tyr165, and Ala167. The sterically disfavored contours (yellow) were all very small for all four CoMFA models, and were located near residues Ile141, Thr147, and Phe142. Although a steric requirement for small molecules with enhanced affinity could be proposed, this is not consistent with the structure–activity relationships of the analogs, as bulky substituents actually decrease inhibition. On the other hand, the electrostatic contour maps agree quite well with the ESP distributions from the DFT calculations. In the red region, negative charges will enhance activity, while positive charges in the blue region favor stronger binding to the enzyme. Despite the fact that the steric contributions dominate according to PLS statistics (ranging from 0.877 to 0.956), we should trust the electrostatic maps more than the steric maps.

To understand the anticancer activities of the compounds in relation to their hydrophobic and H-bonding properties,
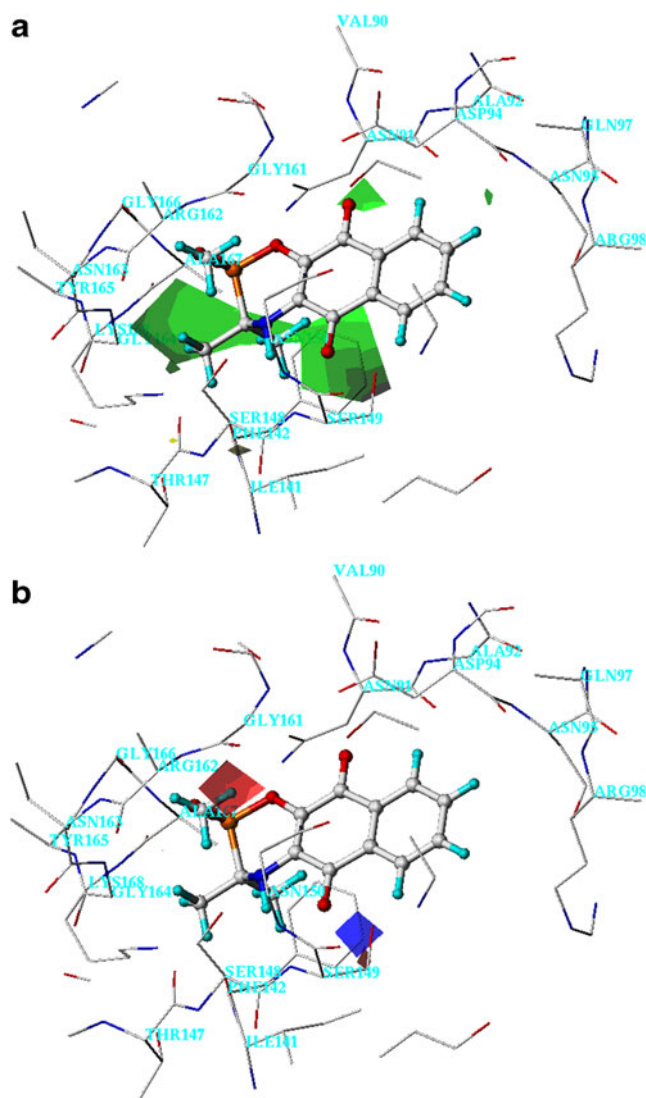

Fig. 6 a–b CoMFA contour maps of A549 activity. Sterically favored regions are shown in *green* and sterically disfavored regions are shown in *yellow* (**a**). Electrostatically favored regions are shown in *blue* and electrostatically disfavored regions are shown in *red* (**b**)

Fig. 7 a–c CoMSIA contour maps of A549 activity. In the hydrophobic contour maps (**a**), the hydrophobic favored maps are shown in *yellow* and the hydrophobic disfavored maps are shown in *gray*. In the H-bond acceptor contour maps (**b**), the H-bond acceptor favored maps are shown in *magenta* and the H-bond acceptor disfavored maps are shown in *red*. In the H-bond donor contour maps (**c**), the H-bond donor favored maps are shown in *cyan* and the hydrophobically disfavored maps are shown in *purple*.

the 3D-QSAR models from the CoMSIA analysis mentioned above were also plotted (Fig. 7). For the hydrophobic contour maps, in the regions with yellow contours, the introduction of more hydrophobic groups leads to stronger inhibition. Yellow contours occur near to Thr147 and Gly164 (Fig. 7a), where hydrophobic contacts are involved (see Fig. 3b). The gray region shows where a less hydrophobic substituent could give better inhibition, and it occurs in a vacant space where no hydrophobic interactions occur. In the H-bond acceptor fields (Fig. 7b), the binding affinity would be enhanced if an H-bond acceptor group on the ligand (or an H-bond donor group on the receptor) was to be introduced into the magenta region. The magenta contours cover a large region, including the space near Ser149 and Ala167, where intermolecular H-bonds are formed and the inhibitor acts as an H-bond acceptor (see Fig. 3a and b). The inhibition would weaken if such a new group was to be placed in the red area. One red area is buried inside the magenta region near residues Phe142 and Ser148, and the other red area is outside the magenta region; neither of them form H-bonds. From the H-bond donor fields (Fig. 7c), introducing an H-bond donor group into the cyan region would increase the cytotoxicity of the compound, while an H-bond donor group in the small purple region would decrease activity. The cyan part in the H-bond donor map is in accord with the red part in the H-bond acceptor map. The small purple contour region is near Ala167, where the inhibitor actually accepts a hydrogen atom instead of donating one. Generally speaking, the hydrophobic and H-bond features were interpreted well based on the suggested binding site from the molecular docking study.

Comparison with other Topo II inhibitor binding models and QSAR studies

Topo II inhibitors can be divided into two classes according to their inhibitory mechanisms: catalytic inhibitors and Topo II poisons [8–15]. For Topo II poisons, the drug interacts directly with DNA; for catalytic inhibitors, the small molecule binds at the ATP-binding site of the Topo II enzyme. The compounds in this paper are thought to be catalytic inhibitors [16, 21]. Goodell et al. [40] have developed a drug–DNA complex model that has provided a new way to comprehend Topo II poisons. On the other hand, in the very first Topo II catalytic inhibitor binding
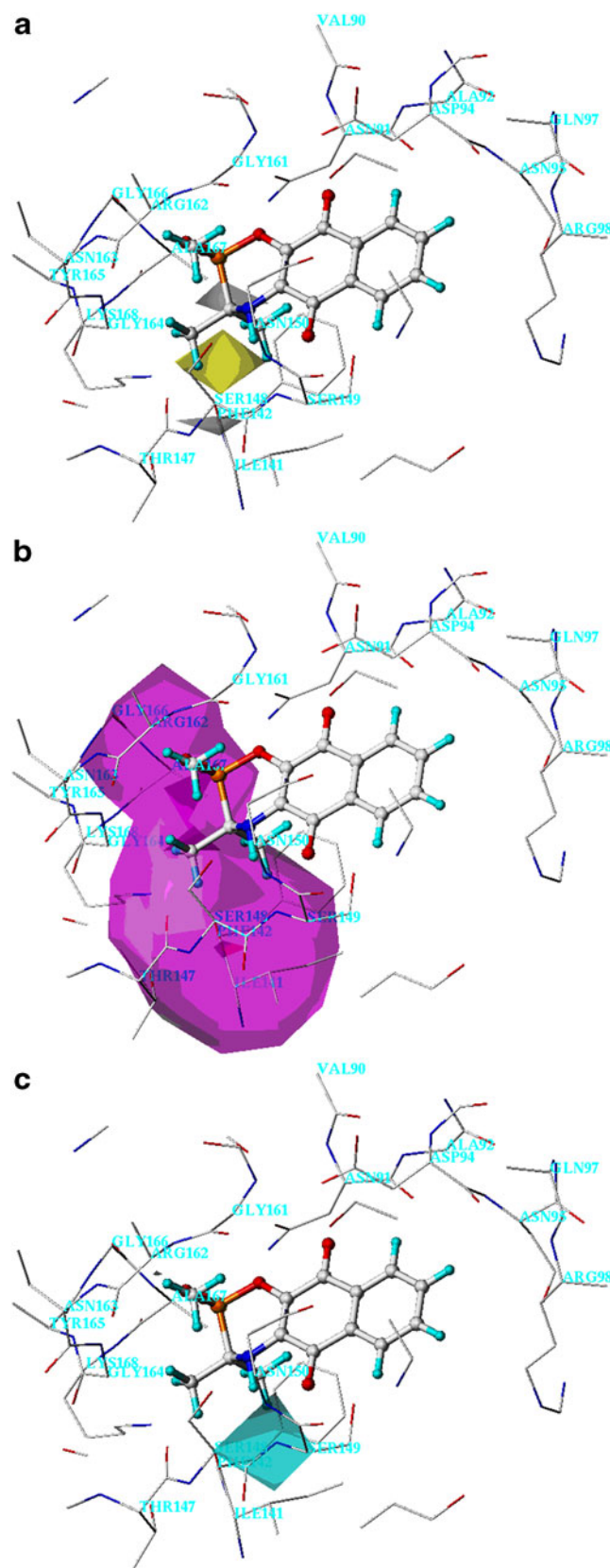
model constructed by Leroy et al., Ser149 and Asn91 were observed to form hydrogen bonds with the inhibitor etoposide [31], and this result is in complete agreement with the binding model reported in our current paper. Very recently, a series of α-heterocyclic carboxaldehyde thiosemicarbazones were reported by Huang et al. to act as Topo II catalytic inhibitors [41]. In that publication, molecular docking was utilized to predict the binding model of the inhibitors. Again, the residue Ser149 formed a hydrogen bond with thiosemicarbazone inhibitor, which indicates that Ser149 may play a very important role when catalytic inhibitors interact with Topo II, and this factor should be taken into account when designing new catalytic inhibitors. If we compare it with the other two models mentioned above [31, 41], we believe that our docking model is fairly successful. In the other three publications about the 3D-QSAR analysis of Topo II inhibitors [14, 17, 18], only CoMFA and CoMSIA contour maps were obtained. Although CoMFA/CoMSIA approaches provide plenty of information on how to design more potent inhibitors, they lack a great deal of important data on the receptor. In our research, 3D-QSAR contour maps were fitted onto the Topo II binding site, which led to a much better understanding the interactions of small inhibitors and macromolecule targets. Thus, we can say that our model of Topo II inhibitors is the most comprehensive one so far.

Conclusions

DNA topoisomerase II is an important target for the design of antitumor drugs, but there are only a few publications that report quantitative structure–activity relationships and the rational design of Topo II inhibitors. Previously a series of naphthoquinone fused cyclic α-aminophosphonates were reported to possess antitumor activities, and they underwent a preliminary assay on Toto II. However, the molecular basis for the activities of these compounds is not available, and structural requirements are also needed in order to design new inhibitors with improved activities. In this paper, we have combined the three popular computational techniques of molecular docking, DFT calculation and CoMFA/CoMSIA methods to predict possible binding modes and to investigate the pharmacophoric requirements of this family of anticancer compounds. We docked the compounds to the active site of the human Topo II structure using the program FlexX, and very reasonable binding modes were obtained. Based on the resulting bioactive conformations, DFT calculations were performed on some compounds in the dataset. Obvious differences were observed between the most potent compounds and less potent compounds in their HOMO distributions. This implies that the molecular frontier orbital may play an

important role in the inhibition of Topo II. The ESPs of the small molecules match quite well with those of the residues of the binding site of Topo II. Furthermore, traditional 3D-QSAR models of CoMFA and CoMSIA were constructed based on four sets of biological activities (A549, HeLa, HEp2 and LoVo) of all of the compounds. High levels of similarity were found among the four CoMFA models, and this suggests that the four different anticancer activities may have the same target. The electrostatic, hydrophobic and H-bond contour maps fit to the binding site of human Topo II perfectly. In conclusion, all of the above results show that our molecular modeling was successful, which not provides computational proof that naphthoquinone fused cyclic α-aminophosphonates are inhibitors of DNA topoisomerase, but they also provide useful guides on the design of new potent compounds for use as Topo II inhibitors in a structure-based approach.

References

1. Trikha M, Corringham R, Klein B, Rossi JF (2003) Targeted anti-interleukin-6 monoclonal antibody therapy for cancer: a review of the rationale and clinical evidence. Clin Cancer Res 9:4653–4665
2. Silvestri GA, Rivera MP (2005) Targeted therapy for the treatment of advanced non-small cell lung cancer: a review of the epidermal growth factor receptor antagonists. Chest 128:3975–3984
3. Langer CJ (2008) Targeted therapy in head and neck cancer: state of the art 2007 and review of clinical applications. Cancer 112:2635–2645
4. William WNJ, Heymach JV, Kim ES, Lippman SM (2009) Molecular targets for cancer chemoprevention. Nat Rev Drug Discov 8:213–225
5. Hightower M (2003) Erlotinib (OSI-774, Tarceva), a selective epidermal growth factor receptor tyrosine kinase inhibitor, in combination with chemotherapy for advanced non-small-cell lung cancer. Clin Lung Cancer 4:336–338
6. Ertongur S, Lang S, Mack B, Wosikowski K, Muehlenweg B, Gires O (2004) Inhibition of the invasion capacity of carcinoma cells by WX-UK1, a novel synthetic inhibitor of the urokinase-type plasminogen activator system. Int J Cancer 110:815–824
7. Hilger RA, Kredke S, Hedley D, Moeller JG, Bauer RJ, Stellberg W, Seeber S, Scheulen ME, Strumberg D (2002) ERK1/2 phosphorylation: a biomarker analysis within a phase I study with the new Raf kinase inhibitor BAY43-9006. Int J Clin Pharmacol Ther 40:567–568
8. Beck WT, Danks MK, Wolverton JS, Granzen B, Chen M, Schmidt CA, Bugg BY, Friche E, Suttle DP (1993) Altered DNA topoisomerase II in multidrug resistance. Cytotechnology 11:115–119
9. Cummings J, Smyth JF (1993) DNA topoisomerase I and II as targets for rational design of new anticancer drugs. Ann Oncol 4:533–543
10. Jensen PB, Sehested M (1997) DNA topoisomerase II rescue by catalytic inhibitors: a new strategy to improve the antitumor selectivity of etoposide. Biochem Pharmacol 54:755–759

11. Wang B, Perchellet EM, Wang Y, Tamura M, Hua DH (2003) Antitumor triptycene bisquinones: a novel synthetic class of dual inhibitors of DNA topoisomerase I and II activities. Anticancer Drugs 14:503–514

12. Meng LH, Ding J (2007) Salvicine, a novel topoisomerase II inhibitor, exerts its potent anticancer activity by ROS generation. Acta Pharmacol Sin 28:1460–1465

13. Rubtsov MA, Terekhov SM, Razin SV, Iarovaia OV (2008) Repositioning of ETO gene in cells treated with VP-16, an inhibitor of DNA-topoisomerase II. J Cell Biochem 104:692–699

14. Temiz-Arpaci O, Tekiner-Gulbas B, Yildiz I, Aki-Sener E, Yalcin I (2005) 3D-QSAR analysis on benzazole derivatives as eukaryotic topoisomerase II inhibitors by using comparative molecular field analysis method. Bioorg Med Chem 13:6354–6359

15. Giles GI, Sharma RP (2005) Topoisomerase enzymes as therapeutic targets for cancer chemotherapy. Med Chem 1:383–394

16. Wang B, Miao ZW, Wang J, Chen RY, Zhang XD (2008) Synthesis and biological evaluation of novel naphthoquinone fused cyclic aminoalkylphosphonates and aminoalkylphosphonic monoester. Amino Acids 35:463–468

17. Liang H, Wu X, Yalowich JC, Hasinoff BB (2008) A three-dimensional quantitative structure–activity analysis of a new class of bisphenol topoisomerase IIalpha inhibitors. Mol Pharmacol 73:686–696

18. Tekiner-Gulbas B, Temiz-Arpaci O, Yildiz I, Aki-Sener E, Yalcin I (2006) 3D-QSAR study on heterocyclic topoisomerase II inhibitors using CoMSIA. SAR QSAR Environ Res 17:121–132

19. Jain HD, Zhang C, Zhou S, Zhou H, Ma J, Liu X, Liao X, Deveau AM, Dieckhaus CM, Johnson MA, Smith KS, Macdonald TL, Kakeya H, Osada H, Cook JM (2008) Synthesis and structure–activity relationship studies on tryprostatin A, an inhibitor of breast cancer resistance protein. Bioorg Med Chem 16:4626–4651

20. Hasinoff BB, Kuschak TI, Yalowich JC, Creighton AM (1995) A QSAR study comparing the cytotoxicity and DNA topoisomerase II inhibitory effects of bisdioxopiperazine analogs of ICRF-187 (dexrazoxane). Biochem Pharmacol 50:953–958

21. Wang B (2007) Design, synthesis and biological activity of novel anthraquinone-phosphorus heterocycles as topo II inhibitors (Ph. D. dissertation). Nankai Univeristy, Tianjin

22. Tripos, Inc. (2004) SYBYL v.6.91. Tripos, Inc., St. Louis

23. Rarey M, Kramer B, Lengauer T, Klebe G (1996) A fast flexible docking method using an incremental construction algorithm. J Mol Biol 261:470–489

24. Cramer M, Cramer RD, Jones DM (1988) Comparative molecular field analysis. 1. Effect of shape on binding of steroids to carrier proteins. J Am Chem Soc 110:5959–5967

25. Klebe G, Abraham U, Mietzner T (1994) Molecular similarity indices in a comparative analysis (CoMSIA) of drug molecules to correlate and predict their biological activity. J Med Chem 37:4130–4146

26. Frisch MJ, Trucks GW, Schlegel HB, Scuseria GE, Robb MA, Cheeseman JR, Montgomery JAJr, Vreven T, Kudin KN, Burant JC, Millam JM, Iyengar SS, Tomasi J, Barone V, Mennucci B, Cossi M, Scalmani G, Rega N, Petersson GA, Nakatsuji H, Hada M, Ehara M, Toyota K, Fukuda R, Hasegawa J, Ishida M, Nakajima T, Honda Y, Kitao O, Nakai H, Klene M, Li X, Knox JE, Hratchian HP, Cross JB, Adamo C, Jaramillo J, Gomperts R, Stratmann RE, Yazyev O, Austin AJ, Cammi R, Pomelli C, Ochterski JW, Ayala PY, Morokuma K, Voth GA, Salvador P, Dannenberg JJ, Zakrzewski VG, Dapprich S, Daniels AD, Strain MC, Farkas O, Malick DK, Rabuck AD, Raghavachari K, Foresman JB, Ortiz JV, Cui Q, Baboul AG, Clifford S, Cioslowski J, Stefanov BB, Liu G, Liashenko A, Piskorz P, Komaromi I, Martin RL, Fox DJ, Keith T, AlLaham MA, Peng CY, Nanayakkara A, Challacombe M, Gill PMW, Johnson B, Chen W, Wong MW, Gonzalez C, Pople JA (2004) Gaussian 03, revision C01. Gaussian, Inc., Wallingford

27. Wei H, Ruthenburg AJ, Bechis SK, Verdine GL (2005) Nucleotide-dependent domain movement in the ATPase domain of a human type IIA DNA topoisomerase. J Biol Chem 280:37041–37047

28. Eldridge MD, Murray CW, Auton TR, Paolini GV, Mee RP (1997) Empirical scoring functions. 1. The development of a fast empirical scoring function to estimate the binding affinity of ligands in receptor complexes. J Comput Aided Mol Des 11:425–445

29. Becke AD (1993) Density-functional thermochemistry. III. The role of exact exchange. J Chem Phys 98:5648–5652

30. Lee C, Yang W, Parr RG (1988) Development of the Colle–Salvetti correlation-energy formula into a functional of the electron density. Phys Rev B 37:785–789

31. Leroy D, Kajava AV, Frei C, Gasser SM (2001) Analysis of etoposide binding to subdomains of human DNA topoisomerase II alpha in the absence of DNA. Biochemistry 40:1624–1634

32. Tripos, Inc. (2003) SYBYL interface to FlexX. Tripos, Inc., St. Louis

33. Wallace AC, Laskowski RA, Thornton JM (1995) LIGPLOT: A program to generate schematic diagrams of protein–ligand interactions. Prot Eng 8:127–134

34. Accelrys, Inc. (2001) ViewerPro 4.2. Accelrys, Inc., San Diego

35. Huang X, Liu T, Gu J, Luo X, Ji R, Cao Y, Xue H, Wong JT, Wong BL, Pei G, Jiang H, Chen K (2001) 3D-QSAR model of flavonoids binding at benzodiazepine site in GABAA receptors. J Med Chem 44:1883–1891

36. Liu XH, Chen PQ, Wang BL, Li YH, Wang SH, Li ZM (2007) Synthesis, bioactivity, theoretical and molecular docking study of 1-cyano-N-substituted-cyclopropanecarboxamide as ketol-acid reductoisomerase inhibitor. Bioorg Med Chem Lett 17:3784–3788

37. Wang JG, Fu XL, Wang YM, Ma Y, Li ZM, Zhang ZX (2003) 3D-QASR Study of quinoline-2,4-dione derivatives against wheat leaf rust. Chem J Chin Univ 24:2010–2013

38. Van DS, Bultinck P (2009) Conceptual DFT properties-based 3D QSAR: analysis of inhibitors of the nicotine metabolizing CYP2A6 enzyme. J Comput Chem 30:1749–1757

39. Schaftenaar G, Noordik JH (2000) Molden: a pre- and post-processing program for molecular and electronic structures. J Comput Aided Mol Des 14:123–134

40. Goodell JR, Ougolkov AV, Hiasa H, Kaur H, Remmel R, Billadeau DD, Ferguson DM (2008) Acridine-based agents with topoisomerase II activity inhibit pancreatic cancer cell proliferation and induce apoptosis. J Med Chem 51:179–182

41. Huang H, Chen Q, Ku X, Meng L, Lin L, Wang X, Zhu C, Wang Y, Chen Z, Li M, Jiang H, Chen K, Ding J, Liu H (2010) A series of alpha-heterocyclic carboxaldehyde thiosemicarbazones inhibit topoisomerase IIalpha catalytic activity. J Med Chem 53:3048–3064